A Rule-Based Energy Management Algorithm for a Fuel Cell/Battery All-Wheel Drive Vehicle

Mario Porru, Alessandro Serpi

Department of Electrical and Electronic Engineering
University of Cagliari
Cagliari, Italy

Novel Electric Propulsion Systems
NEPSY srl
Cagliari, Italy

***Abstract*—An Energy Management Algorithm (EMA) for an All-Wheel Drive (AWD) vehicle is presented in this paper. It consists of a torque vectoring algorithm and a rule-based energy management system for a three-motor fuel cell/battery hybrid road vehicle, which have been developed based on system modelling, operating constraints, and optimisation problem formulation given by the IEEE VTS Motor Vehicle Challenge 2023 (MVC2023). Particularly, the proposed EMA aims at minimising a given cost function, with particular reference to motor and battery losses to extend vehicle driving range at the maximum extent. The proposed EMA is validated through numeric simulations in MATLAB-Simulink, scoring better performances compared to the base EMA provided by the MVC2023.**

Keywords—Energy Management Systems, Hybrid Energy Storage Systems, Optimization, Torque Vectoring

I. INTRODUCTION

Electric Vehicles (EVs) are experiencing a great success on the market over the last years, thanks to important technological improvements that concern their energy storage systems mainly. Nowadays Battery Electric Vehicles (BEVs) are characterized by enough mileage to satisfy the majority of customers, together with a reduced operating cost that quickly pays back the still higher purchase price. In this regard, the increase of battery energy capability per volume/mass unit and the simultaneous reduction of cost per stored kWh have been crucial [1].

Nevertheless, further improvements are desirable in order to make electric vehicles even more competitive with conventional vehicles. For example, enhancing mileage and reducing charging time, as well as increasing safety and stability, are some of the most important aspects that automotive companies have been addressing. Among these, the integration of an hydrogen-based range-extender made up of an hydrogen tank and a fuel cell seems viable as it can provide additional driving miles and could mitigate the range anxiety issue [2]. In addition, hydrogen refuelling process is general faster than battery charging, even when occurring at high power, thus eventually removing the annoying problem of frequent and long charging needs.

Similarly, Electric Propulsion System (EPS) performance can be improved by multi-motor configurations in All-Wheel Drive (AWD) vehicles as using at least one electric motor on both front and rear axles is generally more efficient than single-motor solutions [3]. However, these solutions require dedicated management and control systems to be exploited at the maximum extent. For instance, advanced Energy Management Systems (EMSs) are needed to effectively manage two energy sources on board when Battery Pack (BP) and Fuel Cell (FC) are employed. Several approaches have been proposed over the years, such as simple filter-based EMSs that split high- and low-frequency power components to achieve suitable reference power profiles for BP and FC, respectively [4]. Similarly, rule-based (RB) EMSs can be also employed, which consist of a set of rules established by the human operator that take into account state variables and external conditions to synthesize suitable reference power profiles for BP and FC according to their inherent features [5]. Alternatively, technical and/or economic cost functions can be minimized resorting to look-up tables [6], model predictive control [7], [8], heuristic and/or artificial intelligence techniques [9]. Apart from the EMS, appropriate Torque Vectoring algorithms (TVs) must be employed in AWD vehicles to optimally allocate the total torque demand among the electric motors. Multiple goals may be achieved by appropriate TVs, such as increasing overall efficiency by retrieving energy from both front and rear axle over braking operation [10], as well as by minimizing tire slip losses [11], improving safety, driveability and yaw control [12].

In this context, this paper presents an Energy Management Algorithm (EMA) for a fuel cell/battery hybrid AWD vehicle. Particularly, starting from vehicle modelling, operating constraints and optimisation problem given by the IEEE VTS Motor Vehicle Challenge 2023 (MVC2023) [13], the proposed EMA aims at minimising a given cost function through the employment of both a TV and a RB-EMS. These have been developed mainly to minimise motor and battery losses, respectively, also in accordance with some considerations on the given vehicle configuration, operating constraints, and the technical cost function provided by MVC2023. The proposed EMA is validated through an extensive simulation study carried out in MATLAB-Simulink, which refers to some driving cycles and also to the base EMA provided by MVC2023 for comparison purposes.

II. SYSTEM OVERVIEW

The general overview of the EPS and related control system proposed by the MVC2023 is shown in Fig. 1 [13]. This is split into six main parts, each of which is described in the following:

A. Reference Velocity/Path

This block provides both vehicle reference speed (v^*) and track curvature (ρ^*) over a given driving cycle.

B. Vehicle Control

This block implements both speed and vehicle steering control systems. Particularly, the vehicle reference speed is tracked through a Proportional-Integral (PI) regulator, which

This is the Author's accepted manuscript version of the following contribution:
M. Porru and A. Serpi, "A Rule-Based Energy Management Algorithm for a Fuel Cell/Battery All-Wheel Drive Vehicle," 2023 IEEE Vehicle Power and Propulsion Conference (VPPC), Milan, Italy, 2023, pp. 1-6, doi: 10.1109/VPPC60535.2023.10403350.

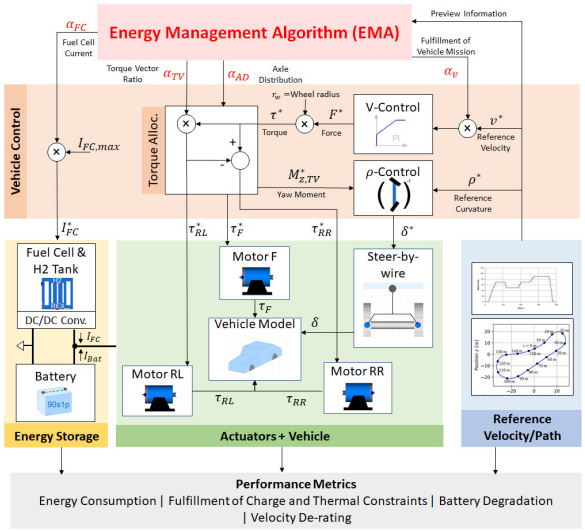

Fig. 1. Schematic overview of the EPS configuration and control system of the AWD vehicle considered for this study [13].

synthesizes the overall reference traction force (F^*), also in accordance with a possible speed derating imposed by EMA through $\alpha_v \in [0,1]$. Given the wheel radius (r_w), F^* is then converted into an equivalent overall torque ($\tau^* = F^* \cdot r_w$), which is split between front (F) and rear (R) axles in accordance with $\alpha_{AD} \in [0,1]$ synthesized by EMA:

$$\tau_F^* = \alpha_{AD}\,\tau^*, \quad \tau_R^* = (1-\alpha_{AD})\,\tau^* . \tag{1}$$

Similarly, overall rear torque is split in accordance with $\alpha_{TV} \in [0,1]$ determined by EMA:

$$\tau_{RR}^* = \alpha_{TV}\,\tau_R^*, \quad \tau_{RL}^* = (1-\alpha_{TV})\,\tau_R^* \tag{2}$$

while the reference FC current is set in accordance with its maximum value and $\alpha_{FC} \in [0,1]$ synthesized by EMA:

$$I_{FC}^* = \alpha_{FC}\, I_{FC}^{(\max)} . \tag{3}$$

C. Actuators + Vehicle

This block simulate electric drives, vehicle dynamic and steering. Particularly, the same Permanent Magnet Synchronous Machine (PMSM) is used for each of the three electric motors installed on board (one on the front axle, two on the rear axle), whose voltage equations in the synchronous dq reference frame can be expressed as

$$\begin{aligned} u_d &= r\,i_d + L\frac{di_d}{dt} - p\omega_m L i_q \\ u_q &= r\,i_q + L\frac{di_d}{dt} + p\omega_m (L i_d + \Lambda) \end{aligned} \tag{4}$$

in which $u_{d/q}$ and $i_{d/q}$ denote the voltage and current space vector components, r and L are the phase resistance and synchronous inductance, respectively, p is the number of pole pairs, ω_m is the electrical rotor speed, and Λ is the equivalent flux-linkage due to permanent magnets. Consequently, the electromagnetic torque developed by each motor is

$$\tau = k_\tau i_q, \quad k_\tau = \frac{3}{2} p\Lambda . \tag{5}$$

Therefore, the overall PMSM power at steady-state operation is

$$P_{PMSM} = \tau\,\omega_m + \frac{3}{2} r\, i_q^2 + \left(k_{hyst} + k_{fric}\right)\omega_m + k_{eddy}\,\omega_m^2 \tag{6}$$

where k_{hyst}, k_{fric}, and k_{eddy} account for hysteresis, friction, and eddy current losses, respectively, while $i_d = 0$ at any operating condition. The power electronic converters have been modelled just considering the corresponding power losses as

$$P_{PEC} = k_0 + k_1\, i_q \tag{7}$$

where k_0 and k_1 are two constant coefficients.

Regarding vehicle modelling, an advanced mechanical and thermal model has been employed, which accounts for longitudinal and lateral motion, tyre losses and the corresponding heat generation, as detailed in [13].

D. Energy Storage

This part consists of an FC and a BP, as highlighted in Fig. 1. The FC is modelled through two look-up tables, which determines H_2 consumption and FC efficiency based on the FC output power [13]. The BP is modelled as a voltage source and an internal series resistance (r_{BP}) so that its output voltage (v_{BP}) can be expressed as

$$v_{BP} = e_{BP} - r_{BP}\, i_{BP} \tag{8}$$

where e_{BP} and i_{BP} denote the BP open-circuit voltage and output current, respectively. It is worth noting that both e_{BP} and r_{BP} depend on BP State-of-Charge (SoC) through suitable look-up tables. Aging phenomenon is also considered, namely BP capacity reduces with average BP current and temperature [13].

E. Energy Management Algorithm

This block implements the strategy that should minimize the following objective function:

$$J = \sum_h k_h \frac{J_h}{J_h^{(0)}}, \quad h \in \{E, SoC, TC, Deg, v, tire\} \tag{9}$$

in which k_h denotes the weighting coefficient of the cost function J_h, while $J_h^{(0)}$ represents its base value, namely the value achieved by the base EMA provided by MVC2023. Particularly, J_E accounts for the overall energy consumption and losses as

$$J_E = \int_0^T \left(p_{FC} + p_{BP} + p_{losses}\right) dt \tag{10}$$

while J_{SoC} is defined as

$$J_{SoC} = \int_0^T 1\big|_{SoC_h \notin \left[SoC_h^{(-)}, SoC_h^{(+)}\right]} dt, \quad h \in \{FC, BP\} . \tag{11}$$

Particularly, J_{SoC} is generally zero but increases when either SoC_{BP} or SoC_{FC} does not lie within their corresponding safe intervals, whose lower and upper thresholds are denoted by $^{(+)}$ and $_{(-)}$, respectively. Additionally, J_{SoC} becomes infinite if any of the following constraints is violated:

$$SoC_h \in \left[SoC_h^{(\min)}, SoC_h^{(\max)}\right], \quad h \in \{FC, BP\} \tag{12}$$

where:

$$SoC_h^{(\min)} < SoC_h^{(-)}, \quad SoC_h^{(+)} < SoC_h^{(\max)} \tag{13}$$

Regarding J_{TC}, this term penalises overcoming BP maximum temperature as follows:

$$J_{TC} = \max_{t}\left\{0, \max\left\{T_{BP} - T_{BP}^{(\max)}\right\}\right\} \quad . \tag{14}$$

Differently, J_{Deg} penalises BP aging as follows:

$$J_{Deg} = \frac{d\Delta Q_{BP}}{dN}, \quad \Delta Q_{BP} = \theta_1 e^{\left(-\frac{\theta_4}{\bar{T}_{BP}} + \left(\theta_2 + \frac{\theta_5}{\bar{T}_{BP}}\bar{I}_{BP}\right)\right)} N^{\theta_3} \tag{15}$$

in which N is the number of BP cycles, ΔQ_{BP} denotes the battery capacity reduction due to aging effects, $\bar{I}_{BP}$ and $\bar{T}_{BP}$ are average BP current and temperature, while $\{\vartheta_1, \vartheta_2, \vartheta_3, \vartheta_4, \vartheta_5\}$ are aging coefficients determined experimentally [13]. In conclusion, J_v and J_{tire} account for possible vehicle speed derating and tire losses, respectively:

$$J_v = \int_0^T (1-\alpha_v)\, dt \,, \quad J_{tire} = \int_0^T p_{tire}\, dt \quad . \tag{16}$$

F. Performance Metrics

This part computes the key performance indexes based on which the effectiveness of the EMA is assessed.

III. EMA DESIGN

A. Design considerations

Given the system modelling resumed by (1)-(8) and the objective function defined by (9)-(16), the EMA should synthesize the most suitable values for α_v, α_{AD}, α_{TV}, and α_{FC}. However, given the complexity of vehicle model and of some of the cost functions, e.g. (15), the proposed EMA has been developed in accordance with the following considerations:

- α_v should be always set at 1 unless SoC_{FC} and SoC_{BP} approaches their corresponding minimum values, in correspondence of which α_v should be nullified to prevent J_{SoC} to become infinite;
- α_{FC} should minimise electrical losses for a given traction power demand. However, BP represents the most critical energy storage unit because it contributes not only to J_E, but also to J_{TC} and J_{Deg}. Consequently, despite sub-optimal, minimising BP usage seems reasonable, meaning that α_{FC} should be synthesized by the RB-EMS directly;
- α_{TV} should minimise J_{tire} in accordance with reference track curvature (ρ^*) and the steering angle (δ^*) determined by the ρ-Control block shown in Fig. 1. However, this approach would be excessively complex, may leading to minor improvements only. Consequently, the relationship suggested by [13] has been employed in this case, namely

$$\alpha_{TV} = 0.5 + k_{TV} \cdot \rho^* \cdot (v^*)^2 \,. \tag{17}$$

Based on the previous considerations, the variables that can be tuned for (9) minimisation purposes are α_{AD} and α_{FC}, which are set by TV and RB-EMS, respectively, as detailed in the following subsections.

B. Torque vectoring

The electric power supplied to each of the three electric drives making up the vehicle EPS can be achieved by combining (5) with (6) and (7) as

$$P_{ED,h} = P_{PMSM,h} + P_{PEC,h} = \frac{3}{2}\frac{r}{k_\tau^2}\tau_h^2 + \left(\omega_{m,h} + \frac{k_1}{k_\tau}\right)\tau_h + p_{0,h} \tag{18}$$

in which $P_{ED,h}$ denotes the overall power supplied to the h-th electric drive, with h ϵ {F,RR,RL), and

$$p_{0,h} = k_{eddy}\,\omega_{m,h}^2 + \left(k_{hyst} + k_{fric}\right)\omega_{m,h} + k_0 \tag{19}$$

Given (1)-(2) and α_{TV}, the overall power demand of the three electric drives can be expressed as a function of α_{AD} as follows

$$P_{ED} = \sum_h P_{ED,h} = p_0 + p_1\alpha_{AD} + p_2\alpha_{AD}^2 \tag{20}$$

in which

$$\begin{aligned} p_0 &= \sum_h p_{0,h} + \tau^*\left(\frac{k_1}{k_\tau} + \omega_{m,RR}\alpha_{TV} + \omega_{m,RL}(1-\alpha_{TV})\right) + \\ &\quad + \frac{3}{2}\frac{r(\tau^*)^2}{k_\tau^2}\left(1 - 2\alpha_{TV} + 2\alpha_{TV}^2\right) \\ p_1 &= \tau^*\left(\omega_F - \omega_{RR}\alpha_{TV} - \omega_{RL}(1-\alpha_{TV}) - \frac{3r\tau^*}{k_\tau^2}\left(1 - 2\alpha_{TV} + 2\alpha_{TV}^2\right)\right) \\ p_2 &= 3\frac{r(\tau^*)^2}{k_\tau^2}\left(1 - \alpha_{TV} + \alpha_{TV}^2\right). \end{aligned} \tag{21}$$

Therefore, minimising (20) leads to

$$\alpha_{AD}^* = \frac{1 - 2\alpha_{TV} + 2\alpha_{TV}^2}{2\left(1 - \alpha_{TV} + \alpha_{TV}^2\right)} - \frac{k_\tau^2}{6r\tau^*}\frac{\left(\omega_F - \omega_{RR}\alpha_{TV} - \omega_{RL}(1-\alpha_{TV})\right)}{\left(1 - \alpha_{TV} + \alpha_{TV}^2\right)} \quad . \tag{22}$$

C. Rule-based EMS

The RB-EMS has been developed to synthesize α_{FC} and α_V that minimize the cost functions of (9) that depend on SoC_{BP} and SoC_{FC}. Particularly, the main goal is managing BP and FC operation within the corresponding safe SoC intervals to avoid cost function penalisation. Hence, the proposed RB-EMS sets α_{FC} and α_V in accordance with a number of operating states and modes, as shown in Fig. 2. Particularly, each operating condition is identified by SoC_{BP} and SoC_{FC} ranges so that the (SoC_{BP}, SoC_{FC}) plane can be split into several regions, each of which corresponds to an operating state (green, yellow, and red areas) and mode, as shown Fig. 2 and resumed in Table I. The NN occurs when both SoC_{BP} and SoC_{FC} lay within their safe operating intervals, so that α_v and α_{FC} can be chosen as

$$\alpha_{FC} = \alpha_{FC}^* = \max\left\{\frac{\sum_h P_{ED,h}}{v_{BP} \cdot I_{FC}^{(\max)}}, 0\right\}, \quad \alpha_V = 1. \tag{23}$$

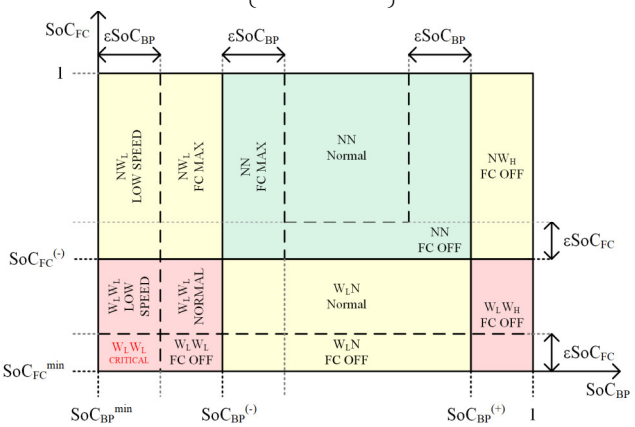

Fig. 2. RB-EMS visual representation: normal (green), single-warning (yellow), and double-warning (red) operating states.

TABLE I. OPERATING STATES AND MODES

Operating States	
-	**Cases**
Normal	NN
Single-warning	W_LN W_HN NW_L
Double-warning	W_LW_L W_HW_L

Operating Modes	
-	**Control actions**
Normal	$\alpha_{FC} = \alpha_{FC}^*$; $\alpha_V = 1$
FC MAX	$\alpha_{FC} = 1$; $\alpha_V = 1$
FC OFF	$\alpha_{FC} = 0$; $\alpha_V = 1$
LOW SPEED	$\alpha_{FC} = \alpha_{FC}^*$; $\alpha_V = 0$
CRITICAL	$\alpha_{FC} = 0$; $\alpha_V = 0$

Given NN, two operating modes can be selected to prevent SoC_{BP} and SoC_{FC} to go outside of their safe operating ranges, which results in increasing J_{SoC} in accordance with (11). Particularly, the FC OFF mode is activated when SoC_{BP} approaches its maximum value or when SoC_{FC} is close to its minimum value as

$$SoC_{BP} > SoC_{BP}^{(+)} - \varepsilon SoC_{BP} \,|\, SoC_{FC} < SoC_{FC}^{(-)} + \varepsilon SoC_{FC} \quad (24)$$

where εSoC_{BP} and εSoC_{FC} define appropriate safety margins within the safe operating region. When FC OFF is active, α_{FC} is nullified, whereas α_V still equals 1 because BP has enough energy to supply the vehicle on its own.

Similarly, the FC MAX operating mode is needed to prevent excessive BP discharging, particularly it is activated when

$$SoC_{BP} < SoC_{BP}^{(-)} + \varepsilon SoC_{BP} \,\&\, SoC_{FC} > SoC_{FC}^{(-)} \quad (25)$$

occurs. In this case, BP exploitation should be minimised and, thus, FC runs at its maximum capability ($\alpha_V = 1$).

Sooner or later SoC_{BP} and/or SoC_{FC} derive from their safe operation intervals due to the inherent vehicle energy consumption, enabling single-warning or double-warning states in case only one SoC or both lie outside their safe operating range, respectively. Considering single-warning states first, three situations may occur depending on which threshold is exceeded. Particularly, NW_H activates when SoC_{BP} is too high:

$$SoC_{BP} > SoC_{BP}^{(+)} \,\&\, SoC_{FC} > SoC_{FC}^{(-)}. \quad (26)$$

If so, BP exploitation should be prioritised and, thus, FC is turned off by selecting the FC OFF mode. Differently, NW_L occurs when SoC_{BP} is too low, and two operating modes are possible. Particularly, when

$$SoC_{BP} > SoC_{BP}^{(\min)} + \varepsilon SOC_{BP} \,\&\, SoC_{FC} > SoC_{FC}^{(-)} \quad (27)$$

FC exploitation is maximised in order to charge BP as much as possible, thus selecting the FC MAX mode. However, if SoC_{BP} decreases further, LOW SPEED mode is enabled to minimise the vehicle consumption by nullifying α_V. The last single-warning state (W_LN) occurs when

$$SoC_{BP} \in \left[SoC_{BP}^{(-)}, SoC_{BP}^{(+)} \right], \quad SoC_{FC} < SoC_{FC}^{(-)} \quad (28)$$

Differently from BP, FC cannot be charged during the driving cycle, so the Normal mode is employed in this case. However, if SoC_{FC} becomes too low, BP exploitation is prioritized to prevent FC to fully discharge, namely FC OFF mode is activated when

$$SoC_{BP} \in \left[SoC_{BP}^{(-)}, SoC_{BP}^{(+)} \right], \quad SoC_{FC} < SoC_{FC}^{(\min)} + \varepsilon SoC_{FC} \quad (29)$$

Double-warning states occur if neither SoC_{BP} nor SoC_{FC} are within their safe operating range, meaning that SoC_{FC} is too low and SoC_{BP} is either too high (W_LW_H) or too low (W_LW_L). In W_LW_H state, BP should be discharged as fast as possible and, thus, FC OFF mode is employed. Alternatively, in W_LW_L state, all four different modes are theoretically possible. However, given that both BP and FC are close to full discharge, Normal mode seems the right choice until

$$SoC_{BP} > SoC_{BP}^{(\min)} + \varepsilon SoC_{BP} \,\&\, SoC_{FC} > SoC_{FC}^{(\min)} + \varepsilon SoC_{FC} \quad (30)$$

When SoC_{BP} becomes too low, namely below the threshold defined in (30), the LOW SPEED mode is imposed. Alternatively, if SoC_{FC} decreases excessively, FC OFF mode is activated. In case both SoC_{BP} and SoC_{FC} are excessively low, the system enter in the CRITICAL mode since both energy storage systems are almost discharged. This imply that both α_{FC} and α_V are nullified to prevent any energy consumption, at least theoretically.

In conclusion, all states, modes and enabled transitions of the proposed RB-EMS are shown in Fig. 3, whereas the presented RB-EMS logic is resumed in Table II.

IV. SIMULATION RESULTS

The proposed EMA has been validated through an extensive simulation study carried out in MATLAB-Simulink by referring to some driving cycles, namely FTP75, Artemis Urban, Artemis Rural, Vires Rural Road Descent 1 and VTS-MVC2023 (a combination of Opt Munchen 2 and FTP75 provided by the MVC organization committee). The simulation setup is still depicted in Fig. 1, whose parameters are omitted for the sake of brevity but can be retrieved from [13]. The operating thresholds of SoC_{BP} and SoC_{FC} are instead resumed in Table III. Results achieved over the Artemis Urban driving cycle are depicted from Fig. 4 to Fig. 7, whereas the final scores of the objective function and of all its components under all the driving cycles considered for this study are resumed in Table IV.

Focusing on Fig. 4 at first, it can be seen that the reference and actual vehicle speed are perfectly superimposed to each other during all the driving cycle, suggesting that the proposed EMA never enters into the LOW SPEED or CRITICAL modes. In addition, power evolutions depicted in Fig. 4 also show that BP slightly assists FC when the latter is on but it handles regenerative braking mainly, whereas BP is capable of propelling the vehicle on its own when FC is off. This is

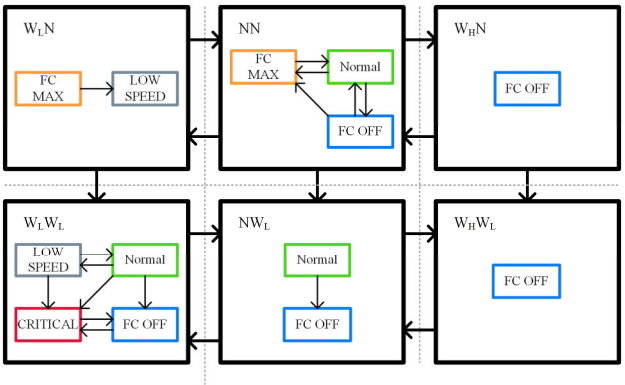

Fig. 3. The proposed RB-EMS state machine and the corresponding states and modes, together with all allowed transitions.

TABLE II. STATE AND MODE SELECTION OF THE PROPOSED RB-EMS

BP & FC SoC States and Modes				State description and goal
BP	***FC***	***State***	***Mode***	
Warning low	Warning low	W_LW_L	Normal	SoC_{BP} and SoC_{FC} are low but normal mode is still available
			FC OFF	SoC_{FC} is approaching its lower limit, so FC is turned off to minimize its usage
			LOW SPEED	SoC_{BP} is approaching its lower limit. Overall consumption is minimized, FC is used to recharge BP
			CRITICAL	SoC_{BP} and SoC_{FC} are too low, so FC is turned off and reference speed is nullified
	Normal	W_LN	FC MAX	SoC_{BP} is low. FC usage is maximise to charge BP
			LOW SPEED	SoC_{BP} is approaching its lower limit. Reference speed is nullified, FC usage is maximised to recharge BP
Normal	Warning low	NW_L	Normal	SoC_{FC} is low but normal operation is possible
			FC OFF	SoC_{FC} is approaching its lower limit. FC is turned off to minimise its usage
	Normal	NN	Normal	SoC_{BP} and SoC_{FC} are within their safe interval
			FC OFF	SoC_{FC} is approaching its lower limit. FC is turned off to minimize its usage
			FC MAX	SoC_{BP} is approaching its lower limit. FC usage is maximized to reduce BP usage
Warning high	Warning low	W_HW_L	FC OFF	SoC_{FC} is low and SoC_{BP} is high. Normal operation is possible, but FC is turned off to maximise BP usage
	Normal	W_HN	FC OFF	SoC_{BP} is high. Normal operation is possible, but FC is turned off to maximize BP usage

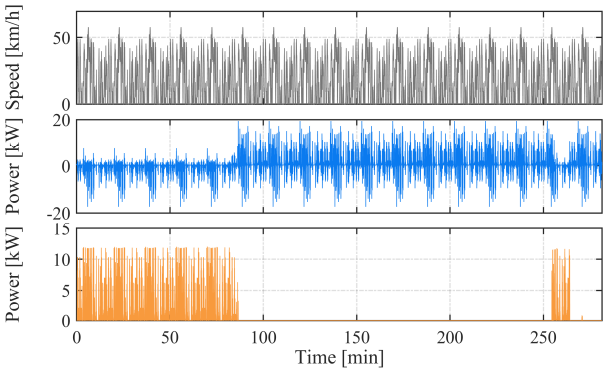

Fig. 4. Reference (black) and actual (gray) vehicle speed (top), battery (blue) and fuel cell (orange) powers achieved over the Artemis Urban driving cycle.

TABLE III. SOC_{BP} AND SOC_{FC} THRESHOLDS

Parameter	Unit	Value
$[SoC_{BP}^{(min)}, SoC_{BP}^{(-)}, SoC_{BP}^{(+)}, SoC_{BP}^{(max)}]$	-	[0.01, 0.20, 0.80,1.00]
$[SoC_{FC}^{(min)}, SoC_{FC}^{(-)}, SoC_{FC}^{(+)}, SoC_{FC}^{(max)}]$	-	[0.01, 0.10, 1.00,1.00]
εSoC_{BP}, εSoC_{FC}	-	0.01

confirmed by the α_V evolution depicted in Fig. 5, in which each colour denotes a different operating mode and which shows that α_V is constantly kept at 1, while α_{TV} and α_{AD} are calculated in accordance with (17) and (22), respectively. Regarding α_{FC}, this shows a less uniform trend, particularly this is computed by (23) in accordance with the Normal operating mode until the event A occurs. After this, α_{FC} is nullified in accordance with FC OFF mode. After approximately 250 minutes, B event occurs, and RB-EMS enables the FC MAX mode and sets α_{FC} to 1 for a very short time interval. Subsequently, Normal and FC OFF modes are activated sequentially after C and D events, respectively.

The RB-EMS operation can be further explained by referring to Fig. 6 and Fig. 7, which show the evolution of SoC_{BP} and SOC_{FC} with time and on the (SoC_{BP}, SOC_{FC}) plane, respectively. It can be seen that SoC_{BP} starts from approximately 0.65, while FC is fully charged, meaning that NN and Normal mode occur first. Therefore, FC is exploited to propel the vehicle, while BP recharges during braking so that SoC_{BP} reaches its

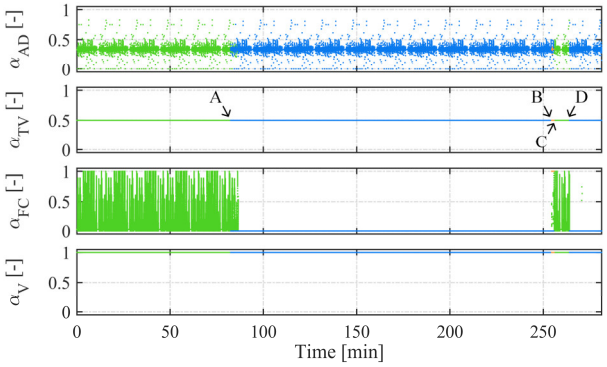

Fig. 5. Evolutions of α control signals during Normal (green), FC OFF (blue), FC MAX (orange), LOW SPEED (gray) and CRITICAL (red) modes achieved over Artemis Urban driving cycle.

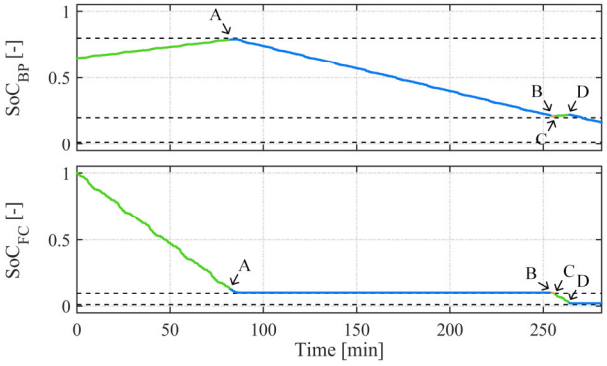

Fig. 6. Evolutions of SoC_{BP} and SoC_{FC} during Normal (green), FC OFF (blue), FC MAX (orange), LOW SPEED (gray) and CRITICAL (red) modes achieved over Artemis Urban driving cycle.

upper threshold ($SoC_{BP}^{(+)}$). When this occurs (event A), FC OFF mode is enabled. Subsequently, Normal and FC OFF modes alternate to each other until FC OFF prevails because SoC_{FC} reaches its lower threshold ($SoC_{FC}^{(-)}$). Consequently, SoC_{FC} maintains constant, whereas BP is gradually discharged until the event B, when the FC MAX mode is activated because SoC_{BP} drops below its lower threshold ($SoC_{BP}^{(-)}$). After a short time

TABLE IV. OBJECTIVE AND COST FUNCTION FINAL SCORES ACHIEVED BY THE PROPOSED RB-EMS (BASE EMA)

Driving Cycle	J	J_E ($J_E^{(0)}$)	J_{SoC} ($J_{SoC}^{(0)}$)	J_{TC} ($J_{TC}^{(0)}$)	J_{Deg} ($J_{Deg}^{(0)}$)	J_v ($J_v^{(0)}$)	J_{tire} ($J_{tire}^{(0)}$)
	[-]	**[kWh]**	**[s]**	**[°C]**	**[Ah/cycle]**	**[s]**	**[Wh]**
Artemis Urban	0.6518	11.44 (11.24)	1.54e3 (15.87e3)	4.25 (5.96)	0.56e-3 (0.61e-3)	0 (0.57e3)	265.08 (227.54)
Artemis Rural	0.6811	2.44 (2.81)	0 (0.19e3)	0 (0)	0.59e-3 (5.01e-3)	0 (0)	13.68 (12.44)
Vires Rural Road Descent 1	0.7720	10.07 (9.30)	0.26e3 (0.74e3)	29.41 (29.50)	0.10 (0.09)	0 (0.08e3)	209.71 (185.15)
VTS-MVC2023	0.7628	11.50 (10.45)	3.05e3 (10.00e3)	8.80 (10.45)	0.70e-3 (0.76e-3)	0.40e3 (1.08e3)	432.93 (417.00)

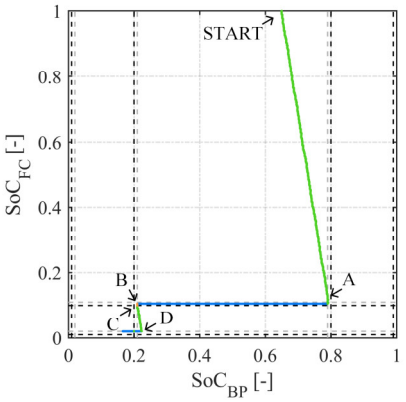

Fig. 7. Trajectory of SoC_{BP} and SoC_{FC} on the (SoC_{BP}, SoC_{FC}) plane achieved over Artemis Urban driving cycle during normal (green), FC OFF (blue), FC MAX (orange), LOW SPEED (gray) and CRITICAL (red) modes.

interval, Normal mode activates again at event C as the system enters into the W_LN state. This results in discharging FC further, whereas BP is slightly recharged. Normal mode is kept until the event D, at which FC OFF mode occurs and this is kept until the end of the driving cycle because SoC_{FC} approaches its minimum threshold ($SoC_{FC}^{(min)}$).

The final scores of all objective function components are resumed in Table IV, together with the corresponding values achieved by the base EMA provided by the MVC2023 organizing committee. In this study, all weighting factors have been assumed equal to 1/6. It can be seen that the proposed EMA is capable of reducing J_{SoC} for all the tested driving cycles, as expected. Furthermore, also J_{TC} and J_v are reduced for all the tested driving cycles, at the cost of an eventual increase of J_E and J_{tire}. Nevertheless, J achieved for all the tested driving cycles is less than 1, highlighting the effectiveness of the proposed EMA.

V. CONCLUSION

This paper has presented an Energy Management Algorithm (EMA) for an All-Wheel Drive fuel cell/battery hybrid electric vehicle equipped with three electric motors used as a benchmark for the IEEE VTS Motor Vehicle Challenge 2023. The proposed EMA consists of a torque vectoring algorithm and a rule-based energy management system, which both aim at minimising a given objective function. Simulation results show that the proposed EMA is generally capable of operating fuel cell and battery within their safe operating ranges, outperforming the base EMA provided by the competition as a benchmark. Future developments will regard a more sophisticated EMA that, for example, takes into account battery temperature control.

REFERENCES

[1] Z. P. Cano *et al.*, "Batteries and fuel cells for emerging electric vehicle markets," *Nat Energy*, vol. 3, no. 4, Art. no. 4, Apr. 2018, doi: 10.1038/s41560-018-0108-1.

[2] M. İnci, M. Büyük, M. H. Demir, and G. İlbey, "A review and research on fuel cell electric vehicles: Topologies, power electronic converters, energy management methods, technical challenges, marketing and future aspects," *Renewable and Sustainable Energy Reviews*, vol. 137, p. 110648, Mar. 2021, doi: 10.1016/j.rser.2020.110648.

[3] C. T. P. Nguyen, J. P. F. Trovao, B.-H. Nguyen, and M. C. Ta, "Powertrain Analysis of an All-Wheel-Drive Off-Road Electric Vehicle," in *2019 IEEE Vehicle Power and Propulsion Conference (VPPC)*, Oct. 2019, pp. 1–6. doi: 10.1109/VPPC46532.2019.8952550.

[4] F. Tao, L. Zhu, Z. Fu, P. Si, and L. Sun, "Frequency Decoupling-Based Energy Management Strategy for Fuel Cell/Battery/Ultracapacitor Hybrid Vehicle Using Fuzzy Control Method," *IEEE Access*, vol. 8, pp. 166491–166502, 2020, doi: 10.1109/ACCESS.2020.3023470.

[5] H.-B. Yuan, W.-J. Zou, S. Jung, and Y.-B. Kim, "A Real-Time Rule-Based Energy Management Strategy With Multi-Objective Optimization for a Fuel Cell Hybrid Electric Vehicle," *IEEE Access*, vol. 10, pp. 102618–102628, 2022, doi: 10.1109/ACCESS.2022.3208365.

[6] A. Serpi and M. Porru, "A Multi-Stage Energy Management System for Multi-Source Hybrid Electric Vehicles," in *Proc. of 45th Annual Conference of the IEEE Industrial Electronics Society (IECON 2019)*, Oct. 2019, pp. 5901–5908. doi: 10.1109/IECON.2019.8926840.

[7] A. Serpi and M. Porru, "An MPC-based Energy Management System for a Hybrid Electric Vehicle," in *Proc. of 2020 IEEE Vehicle Power and Propulsion Conference (VPPC 2020)*, Virtual Conference, Nov. 2020.

[8] C. Jia, W. Qiao, J. Cui, and L. Qu, "Adaptive Model-Predictive-Control-Based Real-Time Energy Management of Fuel Cell Hybrid Electric Vehicles," *IEEE Transactions on Power Electronics*, vol. 38, no. 2, pp. 2681–2694, Feb. 2023, doi: 10.1109/TPEL.2022.3214782.

[9] L. Guo, Z. Li, and R. Outbib, "Reinforcement Learning based Energy Management for Fuel Cell Hybrid Electric Vehicles," in *IECON 2021 – 47th Annual Conference of the IEEE Industrial Electronics Society*, Oct. 2021, pp. 1–6. doi: 10.1109/IECON48115.2021.9589725.

[10] R. de Castro, M. Tanelli, R. E. Araújo, and S. M. Savaresi, "Design of safety-oriented control allocation strategies for overactuated electric vehicles," *Vehicle System Dynamics*, vol. 52, no. 8, pp. 1017–1046, Aug. 2014, doi: 10.1080/00423114.2014.916811.

[11] J. Torinsson, M. Jonasson, D. Yang, and B. Jacobson, "Energy reduction by power loss minimisation through wheel torque allocation in electric vehicles: a simulation-based approach," *Vehicle System Dynamics*, vol. 60, no. 5, pp. 1488–1511, May 2022, doi: 10.1080/00423114.2020.1858121.

[12] B. Lenzo, "Torque Vectoring Control for Enhancing Vehicle Safety and Energy Efficiency," in *Vehicle Dynamics: Fundamentals and Ultimate Trends*, B. Lenzo, Ed., in CISM International Centre for Mechanical Sciences. Cham: Springer International Publishing, 2022, pp. 193–233. doi: 10.1007/978-3-030-75884-4_4.

[13] J. Brembeck, R. De Castro, J. Tobolář, and I. Ebrahimi, "IEEE VTS Motor Vehicles Challenge 2023: A Multi-physical Benchmark Problem for Next Generation Energy Management Algorithms," in *Proc. of 2022 IEEE Vehicle Power and Propulsion Conference (VPPC 2022)*, Nov. 2022, pp. 1–8. doi: 10.1109/VPPC55846.2022.10003375.